THE ASTROPHYSICAL JOURNAL, 494:139–149, 1998 February 10

THE INHOMOGENEOUS JET PARAMETERS IN ACTIVE GALACTIC NUCLEI

D. R. JIANG, XINWU CAO, AND XIAOYU HONG
Shanghai Observatory, Chinese Academy of Sciences, Shanghai, 200030, China; djiang@center.shao.ac.cn
Received 1997 January 27; accepted 1997 September 16

ABSTRACT

The Königl inhomogeneous jet model is applied to investigate the properties of the jets in active galactic nuclei (AGNs). A sample of AGNs that includes measurements of the angular size and radio flux density of the VLBI core, proper motion of the components in the jet, and X-ray flux density is collected. The inhomogeneous jet parameters are derived with the same assumptions for all sources. A comparison among the parameters of different types of sources in the sample is presented. It is found that most of EGRET sources have higher Doppler factors δ, larger Lorentz factors γ, and smaller viewing angles θ as compared to the other sources in the sample. The statistical analyses show that the derived Doppler factor δ is strongly correlated with the observed 22 GHz brightness temperature. Furthermore, there is a correlation between the relative γ-ray luminosity and the Doppler factor δ. The implications of these results are discussed.

Subject headings: galaxies: jets — galaxies: kinematics and dynamics — galaxies: nuclei — gamma rays: observations

1. INTRODUCTION

Superluminal motion has been observed in many active galactic nuclei (AGNs) with VLBI. This provides strong evidence that the plasma in the jets moves at relativistic velocities. In the framework of the unified scheme, the different classes of AGNs (such as radio galaxies, radio-loud quasars, and blazars) can be interpreted as the same kind of source viewed at different directions. Therefore, the bulk velocity in the jets and the viewing angles are two key parameters for understanding the physics of jets and discriminating between models of AGNs.

The energetic γ-ray emissions from AGNs offers an important clue to the physics at work in them. Only one quasar (3C 273) had been detected in high energy γ-ray emission before the launch of EGRET on board the *Compton Gamma-Ray Observatory*. So far, EGRET has detected about 50 AGNs (von Montigny et al. 1995; Thompson et al. 1995). Some interesting results from the observations are (von Montigny et al. 1995):

1. The γ-ray energy flux in many of the sources is dominant over the flux at lower energy bands. The typical isotropic apparent γ-ray luminosities are in the range of 10^{45}–10^{49} ergs s^{-1}.
2. Many of the sources exhibit rapid variability on timescales from days to months, which implies that the size of the emitting region is on the order of the Schwarzschild radius of a black hole with $10^{10}\,M_{\odot}$, under the assumption of isotropic emission.
3. Many active galaxies relatively close to the Earth and some of the superluminal radio sources have not been detected.

The proper-motion measurements in the compact structures of the AGNs provide useful information on the bulk motions of the emitting plasma. In the framework of the relativistic beaming model and the synchrotron self-Compton (SSC) model, the VLBI observations combined with the X-ray flux density could be used to derive the Doppler boosting factor and some physical quantities in the emitting regions of the AGNs. Marscher (1987) derived the beaming parameters on the assumption of a homogeneous spherical emission plasma. Ghisellini et al. (1993) adopted Marscher's approach and obtained the Doppler boosting factor δ for 105 sources. Readhead (1994) suggested estimating the value of the equipartition Doppler boosting factor $\delta_{\rm eq}$ using single-epoch radio data by assuming that the sources are in equipartition between the energy of radiating particles and the magnetic field. Güijosa & Daly (1996) derived $\delta_{\rm eq}$ for the same sample as in Ghisellini et al. (1993). The advantage of the homogeneous sphere model is that the formalism is simple and the value of δ derived is independent of the cosmology model. The component angular size and the flux at the turnover frequency should be known in their calculation. In practice, it is difficult to obtain this information, so one has to assume that the VLBI observing frequency is the synchrotron self-absorption frequency. In addition, the dependence of core size on the observing frequency in some sources is inconsistent with the homogeneous spherical assumption.

Blandford & Königl (1979) and Königl (1981) presented an inhomogeneous relativistic jet model in which both the flat spectrum characteristics of some AGNs and the dependence of the core size on the observing frequency could be well explained. Königl's model involves more free parameters than the homogeneous model, which limits its application. Some authors (Hutter & Mufson 1986; Mufson, Hutter, & Kondo 1989; Unwin et al. 1994; Zensus 1989; Webb et al. 1994) have explored the application of this kind of model to obtain some physical parameters in some sources.

We assemble an AGN sample for which both VLBI and X-ray observations are available. Königl's inhomogeneous jet model is applied in our work to derive the physical parameters of the jets. In § 2, we briefly describe the jet model formalism and the approach. The sample and the results are described in § 3 and § 4, respectively. Section 5 contains a short discussion.

2. MODEL

Königl (1981) proposed an inhomogeneous jet model in which the magnetic field $B(r)$ and the number density of the

relativistic electrons $n_e(r, \gamma_e)$ in the jet are assumed to vary with the distance from the apex of the jet r as $B(r) = B_1(r/r_1)^{-m}$ and $n_e(r, \gamma_e) = n_1(r/r_1)^{-n}\gamma_e^{-(2\alpha+1)}$, respectively, with $r_1 = 1$ pc. If the bulk motion velocity of the jet is βc (corresponding to a Lorentz factor γ) with an opening half-angle ϕ, and the axis of the jet makes an angle θ with the direction of the observer, the distance from the origin of the jet, $r(\tau_{\nu_s} = 1)$, at which the optical depth to the synchrotron self-absorption at the observing frequency ν_s equals unity is given by equation (3) in Königl (1981) as

$$\frac{r(\tau_{\nu_s}=1)}{r_1} = [2c_2(\alpha) r_1 n_1 \phi \csc\theta]^{2/(2\alpha+5)k_m} \times (B_1\delta)^{(2\alpha+3)/(2\alpha+5)k_m}[\nu_s(1+z)]^{-1/k_m}. \quad (1)$$

Here, $c_2(\alpha)$ is the constant in the synchrotron absorption coefficient, δ is the Doppler factor, and $k_m = [2n + m(2\alpha + 3) - 2]/(2\alpha + 5)$. We use the projection of the optically thick region in the jet as a measurement of the observed VLBI core angular size θ_d,

$$\theta_d = \frac{r(\tau_{\nu_s}=1)\sin\theta}{D_a}, \quad (2)$$

where D_a is the angular diameter distance of the source.

By integration of the emission from the optically thick region along the jet, we obtain the radio flux of the core as

$$\begin{aligned} s(\nu_s) &= \frac{1}{4\pi D_a^2}\frac{c_1(\alpha)}{c_2(\alpha)} B_1^{-1/2}\left(\frac{\delta}{1+z}\right)^3\left[\frac{\nu_s(1+z)}{\delta}\right]^{5/2} \\ &\quad \times \int_0^{r(\tau_{\nu s}=1)} 2\left(\frac{r}{r_1}\right)^{m/2}\varphi r\sin\theta\, dr \\ &= \frac{r_1^2\phi\sin\theta}{(4+m)\pi D_a^2}\frac{c_1(\alpha)}{c_2(\alpha)} B_1^{-1/2}\nu_s^{5/2} \\ &\quad \times \left(\frac{\delta}{1+z}\right)^{1/2}\left[\frac{r(\tau_{\nu_s}=1)}{r_1}\right]^{(4+m)/2}, \end{aligned} \quad (3)$$

where ν_s is the VLBI observing frequency, and $c_1(\alpha)$ and $c_2(\alpha)$ are the constants in the synchrotron emission and absorption coefficients, respectively.

Equation (13) in Königl's work gives the X-ray flux density estimation from an unresolved jet. We adopt his expression in the frequency region $\nu_c > \nu_{cb}(r_M)$, where r_M is the smallest radius from which optically thin synchrotron emission with a spectral index α is observed (Königl 1981).

The proper motion observed with VLBI could be converted to the apparent transverse velocity $\beta_{\rm app}$ using the Friedmann cosmology. The apparent transverse velocity $\beta_{\rm app}$ is related to the bulk velocity of the jet βc and viewing angle θ by

$$\beta_{\rm app} = \frac{\beta\sin\theta}{1-\beta\cos\theta}, \quad (4)$$

if the viewing angle θ is available.

The above equations, in conjunction with equation (13) in Königl (1981), can well describe the relation between the physical parameters of the inhomogeneous relativistic jet model and the observational results. The parameters of an inhomogeneous jet could be derived from both VLBI and X-ray observations given the three parameters α, m, n, and the relation between the opening half-angle ϕ and the Lorentz factor γ. The three parameters α, m and n are related to α_{S1}, α_{C2}, and k_m as

$$\alpha_{S1} = \frac{5}{2} - \frac{4+m}{2k_m}, \quad (5)$$

$$\alpha_{C2} = \alpha + \frac{(1+\alpha)m + 2n - 4}{7m-4}, \quad (6)$$

$$k_m = \frac{2n + m(2\alpha+3) - 2}{2\alpha+5}, \quad (7)$$

where α_{S1} is the spectral index of the VLBI core in the radio band, α_{C2} is the spectral index in the X-ray band ($S_\nu \propto \nu^{-\alpha}$), and k_m describes the dependence of the core angular size on the observing frequency ($\theta_d \propto \nu_{\rm ob}^{-1/k_m}$).

In principle, the three parameters α, m, and n could be constrained by the observable quantities α_{S1}, α_{C2}, and k_m. Many researchers have tried to explore the mean value of the spectral index. Padovani, Giommi, & Fiore (1997) suggested that the mean value of the spectral index in the X-ray band of flat-spectrum radio quasars is $\langle\alpha_{\rm X}\rangle \sim 1$. Brunner et al. (1994) obtained $\langle\alpha_{\rm X}\rangle \sim 0.6$ for radio-loud quasars. Lamer, Brunner, & Staubert (1996) found $\langle\alpha_{\rm X}\rangle \sim 1.30$ for BL Lac objects. Padovani & Urry (1992) used $\langle\alpha_{S1}\rangle \sim -0.1$ for flat-spectrum radio quasars. For BL Lac objects, $\langle\alpha_{S1}\rangle \sim -0.3$ is given by Padovani (1992). In cases for which there are multifrequency VLBI observations, $k_m \sim 1$ is found.

Unwin et al. (1994) found $\alpha = 0.6$, $m = 1.5$, and $n = 1.4$ for the conical jet model in 3C 345. The values of k_m, α_{S1}, and α_{C2} in that case are 1.145, -0.1, and 0.78, respectively. These values agree with the statistical values. Hutter & Mufson (1986) expected $m = 1$ and $n = 2$ for a free jet. Webb et al. (1994) derived $m = 0.85$–1.15 and $n = 1.77$–2.4 for 3C 345.

The projection of the opening half-angle $\phi_{\rm ob} = \phi/\sin\theta$ is a measurable quantity. But this kind of information is available only for a few sources. To derive the parameters of the inhomogeneous jet, we have to make some simplified assumptions. Blandford & Königl (1979) suggested $\phi \le 1/\gamma$. Some authors (Hutler & Mufson 1986; Mufson et al. 1989) adopt the assumption $\phi = 1/\gamma$ in their application of this model. Marscher (1987) argues that $\tan\phi = [(3)^{1/2}\gamma]^{-1}$ for a free jet.

In our calculation, we assume $\alpha = 0.75$, $m = 1$, $n = 2$, and the opening half-angle $\phi = 1/\gamma$ in model A, and $\alpha = 0.6$, $m = 1.5$, $n = 1.4$, and $\phi = 1/\gamma$ in model B. The four independent variables n_1, B_1, β, and θ can be derived from equations (2)–(4) and Königl's equation (13) (Königl 1981). Thus we obtain simultaneously the values of the Lorentz factor γ, the viewing angle θ, and the Doppler factor δ.

Equation (1) of Ghisellini et al. (1993),

$$\delta = f(\alpha)F_m\left[\frac{\ln(\nu_b/\nu_m)}{F_{\rm X}\theta_d^{6+4\alpha}\nu_{\rm X}\nu_m^{5+3\alpha}}\right]^{1/(4+2\alpha)}(1+z), \quad (8)$$

is used to compare the results of the homogeneous sphere model, where $F_{\rm X}$ is the X-ray at frequency $\nu_{\rm X}$, and F_m and θ_d are the radio flux density and the angular size, respectively, of the core at the turnover frequency ν_m. The VLBI observing frequency is assumed to be ν_m. We assign the homogeneous sphere model with $\alpha = 0.75$ as model C. The values $H_0 = 75$ km s^{-1} Mpc^{-1} and $q_0 = 0.5$ are used throughout this work.

3. SAMPLE

We have searched the literature for objects that have relevant data, such as the radio flux density, size of the core, proper motion, and X-ray flux density. The VLBI core and X-ray data have been presented by Ghisellini et al. (1993), while Vermeulon & Cohen (1994) have compiled the proper-motion data. The selection criterion of our sample is that all sources have VLBI measurements of the proper motion of outflowing plasma. A total of 52 sources were chosen after a careful literature search, of which 17 are detected EGRET γ-ray sources. The observational data for the sample are presented in Table 1, which gives the redshift (z), VLBI core size (θ_d), and radio flux (S_c) at the frequency ν_s, 1 keV X-ray flux density (S_X), and the proper motion (μ_{app}), with necessary references. The redshift of 0716+714 is not available, and a value of 0.3 is assumed in the calculation. For 1823+568, only the 2 keV X-ray flux density is given, and the 1 keV X-ray flux density was derived by assuming a spectral index of 1.30, which is the average value for BL Lacs. We assume that all the observed X-ray flux

TABLE 1

DATA OF VLBI AND X-RAY OBSERVATIONS

Source	Classification	z	θ_d (mas)	$S_c(\nu_s)$ (Jy)	ν_s (GHz)	Reference	S_X (μJy)	Reference	μ_{app} (mas yr^{-1})	Reference
0016+731	Qc	1.781	0.46	1.58	5.0	1	0.12	1	0.22	2
0106+013	Qc	2.107	0.40	2.30	5.0	1	0.22	1	0.20	2
0133+207	Ql	0.425	0.22	0.082	10.7	3	0.753	4	0.24	2
0153+744	Qc	2.338	0.59	0.64	5.0	1	1.00	1	0.08	2
0208−512[a]	Q	1.003	0.35	2.77	5.0	5	0.08	5	0.60	5
0212+735	Qc	2.367	0.47	1.36	5.0	1	0.23	1	0.09	2
0234+285[a]	Q	1.207	0.1	1.70	22.3	1	0.15	1	0.3	2
0235+164[a]	BL	0.940	0.50	1.75	5.0	1	0.17	1	0.84	6
0316+413	G	0.017	0.30	6.0	22.2	1	18.0	1	0.54	2
0333+321	Qc	1.263	0.33	1.60	3.2	1	1.6	1	0.15	2
0415+379	G	0.0485	0.13	2.9	86.2	7	3.283	4	1.54	2
0420−014[a]	Qc	0.915	0.72	3.43	2.3	1	0.52	1	0.30	8
0430+052	G	0.033	0.40	3.90	5.0	1	10.0	1	2.66	2
0454+844	BL	0.112	0.55	1.3	5.0	1	0.05	1	0.14	2
0528+134[a]	Q	2.070	0.17	0.88	22.2	9	1.59	9	0.5	9
0615+820	Qc	0.710	0.50	0.61	5.0	1	0.20	1	0.05	2
0710+439	Qp	0.518	0.96	0.63	5.0	1	0.55	1	0.04	10
0716+714[a]	BL	0.30	0.35	0.50	5.0	1	0.22	1	0.09	2
0735+178[a]	BL	0.424	0.30	1.29	5.0	1	0.32	1	0.44	2
0836+710[a]	Qc	2.172	0.34	1.05	5.0	1	1.0	1	0.23	2
0850+581	Qc	1.322	0.48	0.94	5.0	1	0.97	1	0.12	2
0851+202	BL	0.306	0.30	2.30	5.0	1	1.70	1	0.27	2
0906+430	Qcl	0.670	0.104	0.875	5.0	1	0.09	1	0.18	2
0917+624	Q	1.446	0.115	1.22	8.4	11	0.12	11	0.23	11
0923+392	Qc	0.699	0.69	6.90	5.0	1	0.37	1	0.18	2
0954+658[a]	BL	0.368	0.19	0.477	5.0	18	0.5	1	0.44	19
1040+123	Qcl	1.029	0.33	0.59	10.7	1	0.121	1	0.11	2
1101+384[a]	BL	0.031	0.30	0.24	5.0	1	14.0	1	1.33	2
1150+812	Qc	1.250	0.50	0.46	5.0	1	0.20	1	0.11	2
1156+295[a]	Q	0.729	0.123	1.40	22.2	1	0.15	1	1.15	2
1219+285[a]	BL	0.102	0.20	0.159	5.0	19	0.42	1	0.55	19
1226+023[a]	Qc	0.158	0.14	3.49	15.0	1	21	1	1.20	2
1228+127	G	0.0032	0.70	1.0	5.0	1	0.68	1	3.07	12
1253−055[a]	Qc	0.538	0.14	4.84	15.0	1	1.4	1	0.50	2
1308+326	BL	0.996	0.50	1.97	5.0	1	0.30	1	0.75	2
1618+177	Ql	0.555	0.20	0.086	10.7	1	0.3	1	0.10	2
1633+382[a]	Qc	1.814	0.15	5.4	10.7	13	0.08	14	0.16	10
1637+826	G	0.023	0.20	0.67	10.7	1	0.30	1	0.3	15
1641+399	Qc	0.595	0.30	6.90	22.0	1	0.66	1	0.47	2
1721+343	Ql	0.2055	0.24	0.109	10.7	1	1.9	1	0.28	2
1749+701	BL	0.770	0.39	0.22	5.0	1	0.22	1	0.26	2
1803+784	BL	0.684	0.20	1.436	5.0	18	0.16	1	0.004	2
1807+698?.....	BL	0.051	0.79	0.95	5.0	1	0.60	1	2.6	16
1823+568	BL	0.664	0.35	1.132	5.0	10	0.2	10	0.12	2
1845+797	Ql	0.057	0.50	0.31	5.0	1	1.1	1	0.37	17
1928+738	Qc	0.302	0.49	2.11	5.0	1	0.55	1	0.60	2
2007+776	BL	0.342	0.19	1.361	5.0	19	0.11	1	0.18	2
2134+004	Qc	1.936	0.62	6.7	5.0	1	0.04	1	0.01	15
2200+420	BL	0.069	0.35	1.60	5.0	1	0.82	1	1.2	2
2223−052	Qc	1.404	0.10	1.98	15.0	1	1.1	1	0.06	2
2230+114[a]	Qp	1.037	0.50	0.54	5.0	1	0.34	1	0.5	2
2251+158[a]	Qc	0.859	0.30	0.90	5.0	1	0.56	1	0.35	2

[a] EGRET sources: Q: quasar; Qc: core-dominated quasar; Ql: lobe-dominated quasar; Qp: GHz peaked quasar; G: Galaxy.

REFERENCES.—(1) Ghisellini et al. 1993; (2) Vermeulen & Cohen 1994; (3) Vermeulen et al. 1993; (4) Wilkes et al. 1994; (5) Shen 1996; (6) Chu et al. 1996; (7) Doeleman, Rogers, & Moran 1994; (8) Krichbaum et al. 1994; (9) Zhang et al. 1994; (10) Pearson & Readhead 1988; (11) Rantakyrö et al. 1996; (12) Biretta, Zhou, & Owen 1995; (13) Kellermann et al. 1977; (14) Ku, Helfand, & Lucy 1980; (15) Zensus 1989; (16) Mutel 1990; (17) Porcas 1987; (18) Gabuzda et al. 1992; (19) Gabuzda et al. 1994.

density is attributable to the SSC emission in the derivation, which will result in some uncertainties. In addition, the X-ray observations are not contemporaneous with the VLBI observations, which will also introduce some uncertainties. However, our calculations show that the value of the X-ray flux density is not sensitive to the derived parameters. Another uncertainty of the data is the proper motion. We assume the fastest one when there are more than one moving components. Even though it is not quite certain that the observed proper motion could represent real information on the core, we think that the observed proper motion is a good approximation.

4. RESULTS

Using the method described in § 2, the jet parameters for all the sources in our sample are derived. The results are shown in Table 2 for the above models A and B. We note that there are no large differences between the results from these two models, so we will discuss only model A for comparison to the homogeneous model (model C).

4.1. *Distribution of Doppler Factor and Lorentz Factor*

In Figure 1 we show the distribution of the derived Doppler factor δ for the 17 EGRET sources and the 45 remaining sources in our sample. The EGRET sources have higher values of δ, except three BL Lacs: 0716+714, 1101+384 (Mrk 421), and 1219+285. The distributions of the Lorentz factor γ are plotted in Figure 2. Similarly, it is found that the EGRET sources have relatively high values of γ. From Figures 1 and 2 we note that there are some objects with high values of δ or γ that have not been measured in γ-radiation by EGRET. Compared with the other EGRET sources, three BL Lacs, 0716+714, Mrk 421, and 1219+285, have relatively low values of both δ and γ. The BL Lac object Mrk 421 is special because of its detection as a TeV source as well as an EGRET source. The redshift of object 0716+714 is not available, so we have assumed a value of 0.3, which probably increases the uncertainty of its derived parameters. These three objects show interesting characteristics.

Figure 3*a* plots the Lorentz factors γ for all the objects in our sample with $\delta > \delta_c$, where $\delta_c = 4.5$ for model A. The 14 EGRET sources show large values of the Lorentz factor γ, with $\gamma \geq 10$. Similar phenomena are shown for model B, where $\delta_c = 3.5$. Almost all of the remaining objects with $\delta > \delta_c$ show relatively lower Lorentz factors γ, except the source 1308+326. Figure 3*b* shows the results for model C, which has $\delta_c = 2.5$.

The statistical information on the Doppler factor δ, Lorentz factor γ, and the viewing angle θ for the different classes of sources in our sample are listed in Table 3. In Figure 4, the Lorentz factor γ is mapped against the viewing angle θ for all sources.

4.2. *Distribution of Turnover Frequency*

In our model, the observed turnover frequency ν_{sM} of the radio continuum could be naturally derived. If there are enough dedicated measurements of the turnover frequency, it will offer an effective examination of our model. Estimates of the synchrotron self-absorption frequency for some sources (Bloom et al. 1994; Reich et al. 1993) seem to be compatible with our results. We depict the distribution of the turnover frequency in the source rest frame $(1 + z)\nu_{sM}$ in Figure 5. The EGRET sources have relatively higher turnover frequencies, as measured in the source rest frame, as compared to the other sources in our sample. This could be a natural result of the fact that the EGRET sources have high Doppler factor (see § 4.1). No obvious differences are found in the intrinsic turnover frequencies $[\nu_{sM}(1 + z)/\delta]$ between the EGRET and other sources in our sample.

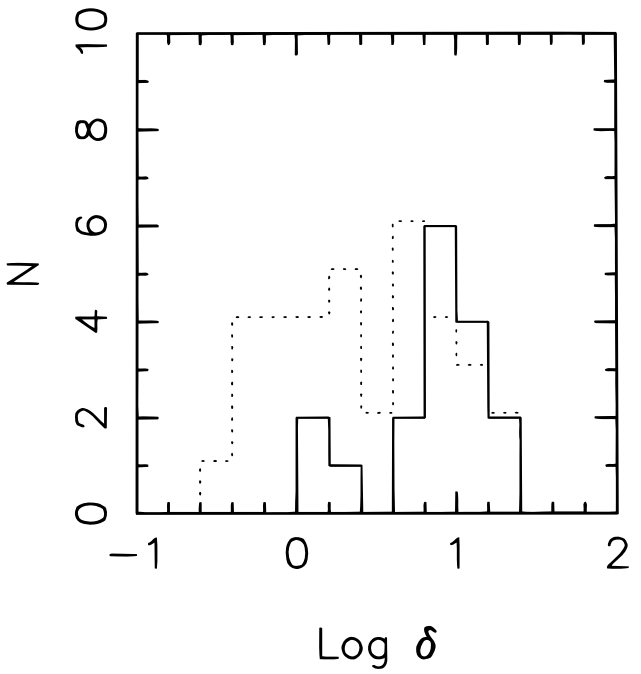

FIG. 1*a*

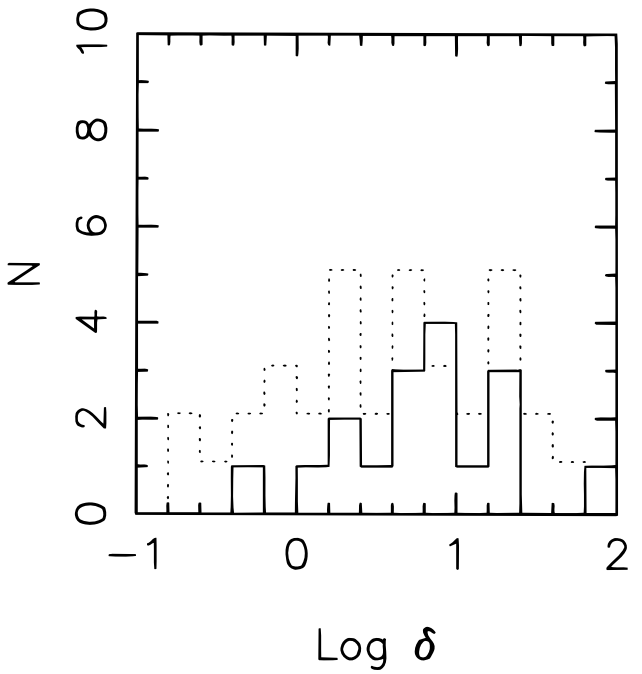

FIG. 1*b*

FIG. 1.—Distributions of the Doppler factor δ for the EGRET sources (*solid histograms*) and the rest of the sources in the sample (*dotted histograms*) derived from (*a*) model A and (*b*) model C, respectively.

TABLE 2

DERIVED JET PARAMETERS FOR MODELS A AND B

Source	Classification	θ (deg)	γ	δ	B_1 (gauss)	n_1 (cm^{-3})	ν_{sM} (GHz)
			Model A				
0016+731	Qc	6.6	11.7	8.3	3.85E−01	7.88E+05	2.3E+02
0106+013	Qc	4.7	11.1	12.2	3.63E−01	6.34E+04	2.6E+02
0133+207	Ql	22.6	20.5	0.6	1.64E−01	1.21E+06	2.8E+02
0153+744	Qc	20.6	6.3	2.1	1.95E−01	1.18E+06	1.0E+02
0208−512[a].....	Q	2.6	22.3	21.7	5.07E−01	1.10E+04	7.9E+02
0212+735	Qc	11.8	5.3	4.9	2.33E−01	1.63E+05	1.4E+02
0234+285[a].....	Q	6.2	13.3	8.7	3.63E−01	4.98E+04	3.7E+02
0235+164[a].....	BL	3.3	42.1	12.6	6.79E−01	6.43E+04	8.0E+02
0316+413	G	93.2	1.2	0.8	1.10E−02	4.40E+03	2.2E+02
0333+321	Qc	4.0	7.7	11.9	1.44E−01	2.88E+04	7.8E+02
0415+379	G	24.1	15.0	0.7	1.58E−01	1.65E+05	2.6E+02
0420−014[a].....	Qc	3.7	11.2	14.8	2.69E−01	1.81E+04	7.3E+02
0430+052	G	7.4	5.8	7.4	2.45E−02	3.52E+02	2.8E+03
0454+844	BL	51.3	1.4	1.3	4.14E−02	2.90E+03	7.7E+01
0528+134[a].....	Q	4.1	73.0	5.2	9.11E−01	3.70E+06	3.4E+01
0615+820	Qc	51.1	2.0	1.1	8.76E−02	1.16E+05	5.9E+01
0710+439	Qp	89.3	3.0	0.3	1.45E−01	1.76E+06	3.0E+01
0716+714[a].....	BL	44.9	1.8	1.4	4.33E−02	1.42E+04	1.3E+02
0735+178[a].....	BL	7.0	9.1	8.1	1.41E−01	7.09E+03	7.9E+02
0836+710[a].....	Qc	5.7	13.3	9.8	2.37E−01	1.31E+05	5.1E+02
0850+581	Qc	16.2	6.1	3.1	1.65E−01	2.39E+05	1.9E+02
0851+202	BL	8.1	4.7	6.5	7.93E−02	6.84E+03	7.7E+02
0906+430	Qcl	1.9	9.2	16.7	1.51E−01	2.06E+03	1.2E+03
0917+624	Q	2.8	12.0	17.7	2.53E−01	1.07E+04	7.0E+02
0923+392	Qc	9.4	5.4	6.1	2.85E−01	4.22E+04	1.8E+02
0954+658[a].....	BL	8.0	8.2	7.1	7.41E−02	4.33E+03	1.3E+03
1040+123	Qcl	24.7	7.4	1.4	2.82E−01	5.04E+05	7.3E+01
1101+384[a].....	BL	35.2	3.5	1.3	7.68E−03	1.58E+03	1.8E+03
1150+812	Qc	21.0	6.8	1.9	2.01E−01	2.98E+05	1.1E+02
1156+295[a].....	Q	3.0	63.1	10.5	8.24E−01	8.66E+04	9.2E+02
1219+285[a].....	BL	24.8	3.9	2.1	2.12E−02	1.40E+03	8.8E+02
1226+023[a].....	Qc	6.3	11.0	8.9	7.18E−02	8.09E+03	2.4E+03
1228+127	G	89.0	1.3	0.8	3.79E−03	5.39E+01	4.1E+02
1253−055[a].....	Qc	4.2	12.3	13.5	2.34E−01	1.64E+04	8.5E+02
1308+326	BL	3.4	36.7	12.6	5.96E−01	7.43E+04	8.2E+02
1618+177	Ql	42.1	7.4	0.5	1.11E−01	6.67E+05	1.0E+02
1633+382[a].....	Qc	1.9	12.1	21.0	5.77E−01	2.27E+04	3.3E+02
1637+826	G	79.7	1.1	1.0	6.85E−03	4.50E+02	1.9E+02
1641+399	Qc	8.1	19.2	4.6	6.85E−01	3.14E+05	2.1E+02
1721+343	Ql	34.4	11.7	0.5	8.07E−02	4.97E+05	3.1E+02
1749+701	BL	13.1	16.8	2.2	2.22E−01	2.20E+05	3.2E+02
1803+784	BL	10.3	1.1	1.5	6.31E−02	8.08E+04	3.7E+01
1807+698	BL	13.3	17.2	2.0	9.82E−02	8.28E+03	8.1E+02
1823+568	BL	15.6	3.6	3.7	1.15E−01	2.05E+04	2.0E+02
1845+797	Ql	69.0	2.5	0.6	2.05E−02	9.33E+03	2.6E+02
1928+738	Qc	8.7	10.4	6.0	1.69E−01	1.37E+04	6.5E+02
2007+776	BL	5.5	4.5	7.5	1.01E−01	2.02E+03	5.3E+02
2134+004	Qc	11.6	1.5	2.4	3.12E−01	2.19E+05	1.4E+01
2200+420	BL	11.0	5.1	5.2	3.92E−02	6.40E+02	1.2E+03
2223−052	Qc	8.3	3.5	5.5	1.30E−01	6.89E+04	2.1E+02
2230+114[a].....	Qp	5.7	40.7	4.7	5.10E−01	3.74E+05	6.4E+02
2251+158[a].....	Qc	6.5	12.6	8.2	1.84E−01	3.12E+04	7.8E+02
			Model B				
0016+731	Qc	7.3	12.3	7.2	1.18E+00	7.98E+03	7.7E+01
0106+013	Qc	5.6	11.0	10.3	1.00E+00	7.04E+03	9.7E+01
0133+207	Ql	22.7	24.3	0.5	1.79E−01	4.86E+05	1.2E+02
0153+744	Qc	21.3	6.8	1.9	4.75E−01	1.15E+05	4.0E+01
0208−512[a].....	Q	3.3	23.2	16.9	1.33E+00	2.17E+03	2.3E+02
0212+735	Qc	12.7	5.3	4.5	6.53E−01	1.22E+04	4.0E+01
0234+285[a].....	Q	6.5	13.6	8.1	7.39E−01	6.03E+03	1.3E+02
0235+164[a].....	BL	3.5	52.0	9.5	2.19E+00	1.51E+04	2.5E+02
0316+413	G	98.5	1.3	0.7	3.40E−03	4.76E+03	9.7E+01
0333+321	Qc	6.3	6.7	8.7	1.74E−01	1.05E+04	2.4E+02
0415+379	G	24.1	14.5	0.8	1.07E−01	3.97E+04	1.3E+02
0420−014[a].....	Qc	5.3	10.6	10.9	5.61E−01	4.36E+03	2.0E+02
0430+052	G	11.7	5.5	4.9	5.63E−03	1.90E+03	9.4E+02
0454+844	BL	53.0	1.4	1.2	4.81E−02	5.27E+02	2.7E+01
0528+134[a].....	Q	4.1	84.0	4.5	2.38E+00	5.09E+05	2.2E+02

TABLE 2—*Continued*

Source	Classification	θ (deg)	γ	δ	B_1 (gauss)	n_1 (cm^{-3})	ν_{sM} (GHz)
0615+820	Qc	52.0	2.1	1.1	1.68E−01	1.05E+04	2.3E+01
0710+439	Qp	89.2	2.9	0.3	3.78E−01	7.76E+04	1.3E+01
0716+714[a].....	BL	49.0	1.8	1.2	4.46E−02	4.07E+03	4.7E+01
0735+178[a].....	BL	8.7	9.8	6.2	1.74E−01	3.68E+03	2.5E+02
0836+710[a].....	Qc	6.6	14.6	7.6	4.43E−01	3.66E+04	1.7E+02
0850+581	Qc	17.4	6.6	2.7	3.34E−01	3.98E+04	7.1E+01
0851+202	BL	11.5	4.4	5.0	6.73E−02	3.91E+03	2.4E+02
0906+430	Qcl	3.2	7.4	12.6	1.39E−01	8.84E+02	3.3E+02
0917+624	Q	3.8	11.1	14.5	3.76E−01	2.55E+03	2.3E+02
0923+392	Qc	10.7	5.4	5.4	9.06E−01	3.21E+03	6.1E+01
0954+658[a].....	BL	10.2	9.1	5.1	5.25E−02	5.78E+03	4.1E+02
1040+123	Qcl	24.7	7.3	1.4	7.20E−01	2.71E+04	3.0E+01
1101+384[a].....	BL	39.3	4.8	0.9	1.21E−03	2.60E+04	6.6E+02
1150+812	Qc	21.5	7.3	1.7	4.71E−01	3.28E+04	4.3E+01
1156+295[a].....	Q	3.1	73.3	8.8	1.92E+00	1.82E+04	3.5E+02
1219+285[a].....	BL	28.4	4.6	1.5	7.22E−03	4.75+03	3.0E+02
1226+023[a].....	Qc	7.9	12.4	6.3	3.63E−02	1.75E+04	1.0E+03
1228+127	G	102.6	1.5	0.6	5.90E−04	4.13E+02	1.3E+02
1253−055[a].....	Qc	5.2	12.4	11.0	3.17E−01	5.30E+03	3.6E+02
1308+326	BL	3.7	45.1	9.5	1.81E+00	1.87E+04	2.6E+02
1618+177	Ql	42.3	7.9	0.5	1.26E−01	1.40E+05	5.3E+01
1633+382[a].....	Qc	2.2	11.3	18.9	1.92E+00	1.44E+03	1.1E+02
1637+826	G	95.0	1.1	0.9	1.86E−03	6.71E+02	7.3E+01
1641+399	Qc	8.2	19.8	4.4	2.27E+00	1.81E+04	9.5E+01
1721+343	Ql	34.7	14.0	0.4	5.87E−02	3.47E+05	1.4E+02
1749+701	BL	13.4	20.4	1.7	4.01E−01	6.71E+04	1.2E+02
1803+784	BL	10.2	1.1	1.5	1.82E−01	3.56E+03	1.5E+01
1807+698	BL	13.6	22.6	1.5	7.89E−02	1.20E+04	2.7E+02
1823+568	BL	17.9	3.6	3.2	1.90E−01	3.65E+03	6.8E+01
1845+797	Ql	71.4	3.0	0.5	9.39E−03	1.33E+04	9.7E+01
1928+738	Qc	9.8	12.0	4.6	2.58E−01	6.05E+03	2.1E+02
2007+776	BL	7.8	3.9	6.1	1.02E−01	6.92E+02	1.6E+02
2134+004	Qc	9.2	1.6	2.7	3.14E+00	1.83E+03	5.4E+00
2200+420	BL	14.6	5.3	3.8	1.72E−02	1.30E+03	3.7E+02
2223−052	Qc	9.4	3.4	5.1	1.97E−01	9.26E+03	9.1E+01
2230+114[a].....	Qp	5.8	51.7	3.6	1.38E+00	9.79E+04	1.9E+02
2251+158[a].....	Qc	7.6	14.4	6.2	2.77E−01	1.47E+04	2.5E+02

[a] EGRET source.

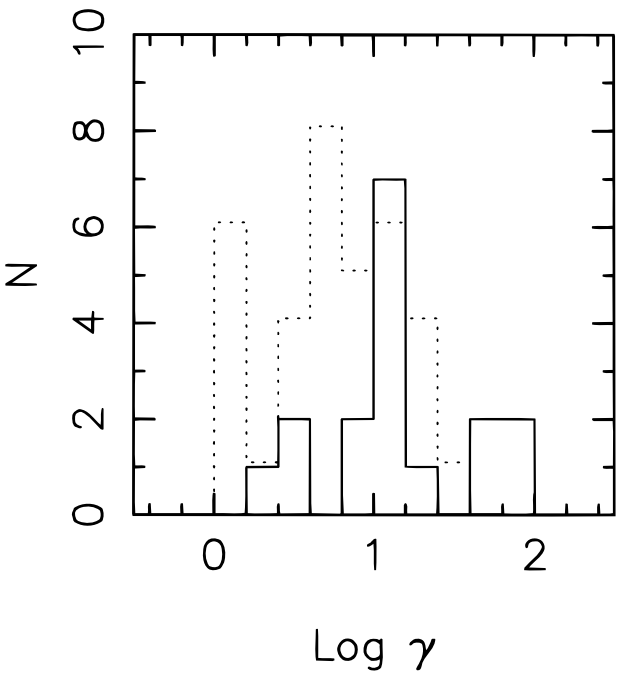

FIG. 2*a*

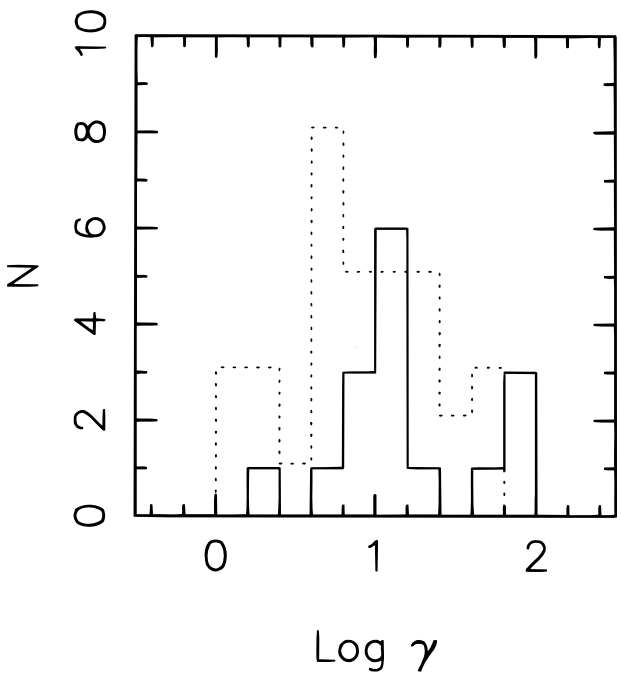

FIG. 2*b*

FIG. 2.—Distributions of the Lorentz factor γ, representations as in Fig. 1

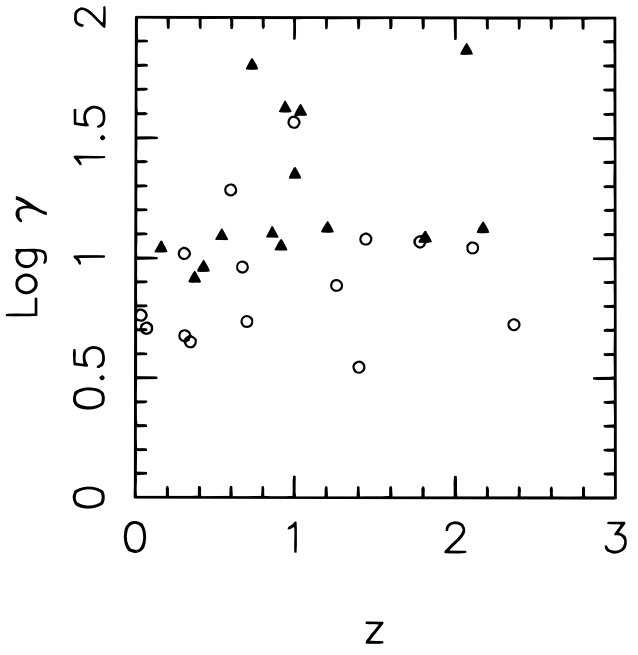

FIG. 3*a*

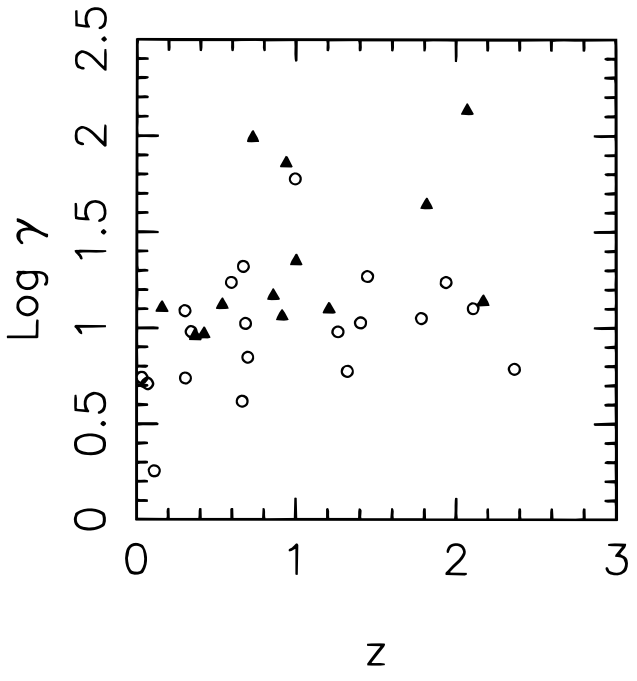

FIG. 3*b*

FIG. 3.—Lorentz factor γ for sample sources with Doppler factor $\delta > \delta_c$, for (*a*) model A and (*b*) model C, respectively. *Triangles*: EGRET sources; *circles*: all other sources.

4.3. *Correlation of Brightness Temperature* $(1 + z)T_b$ *in the Source Rest Frame with Doppler Factor* δ

In Figure 6*a* and 6*b*, we plot the brightness temperature in the source rest frame $(1 + z)T_b$ against the Doppler factor δ derived from models A and C, respectively. The observed 22 GHz brightness temperatures T_b are taken from Moellenbrock et al. (1996). The total number of sources is 31, of which only 13 have low limits on the brightness temperature. There are significant correlations (at 99.9% for both models A and B) between the brightness temperature in the source rest frame and the Doppler factor derived from the model. In calculating the correlation, the source 0016+731 is not included, as the brightness temperature of this source is only given a lower limit. The best correlations for the data derived from models A and B are $\log (1 + z)T_b = 10.98 + 0.84 \log \delta$ and $\log (1 + z)T_b = 11.00 + 0.93 \log \delta$, respectively. A less significant correlation is found for model C, $\log (1 + z)T_b = 11.22 + 0.45 \log \delta$ (for a correlation coefficient $r = 0.39$, at the 98% confidence level). The correlation derived from our model seems to agree with the prediction: $(1 + z)T_b \propto \delta$.

TABLE 3

MEAN VALUES

Source	N	Model	δ	θ	γ
All	52	A	6.2	20.5	12.3
		B	5.0	22.3	13.7
BL Lacs.....	15	A	5.0	17.0	10.6
		B	3.9	19.0	12.6
Qc[a]	26	A	8.8	9.8	14.2
		B	7.2	10.6	15.3
Ql	4	A	0.6	42.0	10.5
		B	0.5	42.8	12.3
G	5	A	2.1	58.7	4.9
		B	1.6	66.4	4.8

[a] Five Q are included in Qc.

The correlation between the values of the Doppler factor δ derived from models A and C is shown in Figure 7. A good correlation is found, which means that the statistical behavior of the Doppler factor derived from a homogeneous sphere model shows no significant difference from our model. Nonetheless, the values of the Lorentz factor γ derived in the homogeneous sphere model for some sources would be as high as several hundred, mainly because of the extremely low estimate of the Doppler factor for these

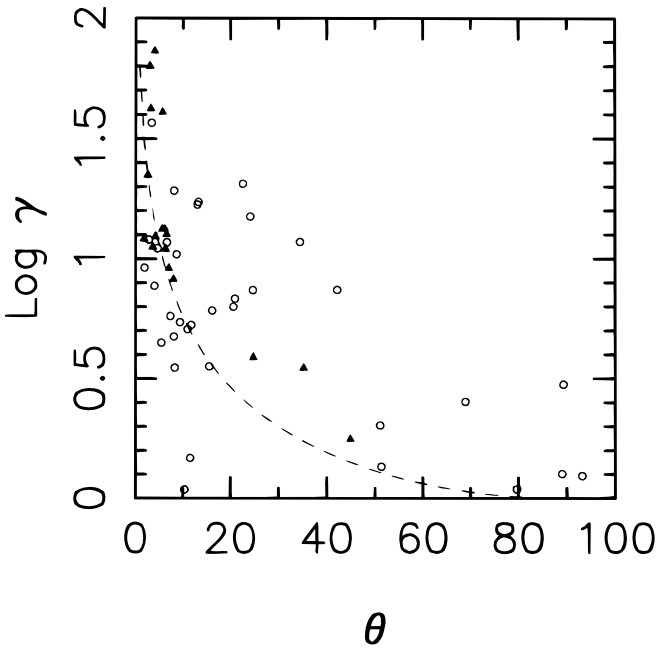

FIG. 4.—Lorentz factor γ vs. viewing angle θ for all sources in the sample, derived from model A. *Triangles*: EGRET sources; *circles*: all other sources. Dashed line represents $\gamma = 1/\sin \theta$.

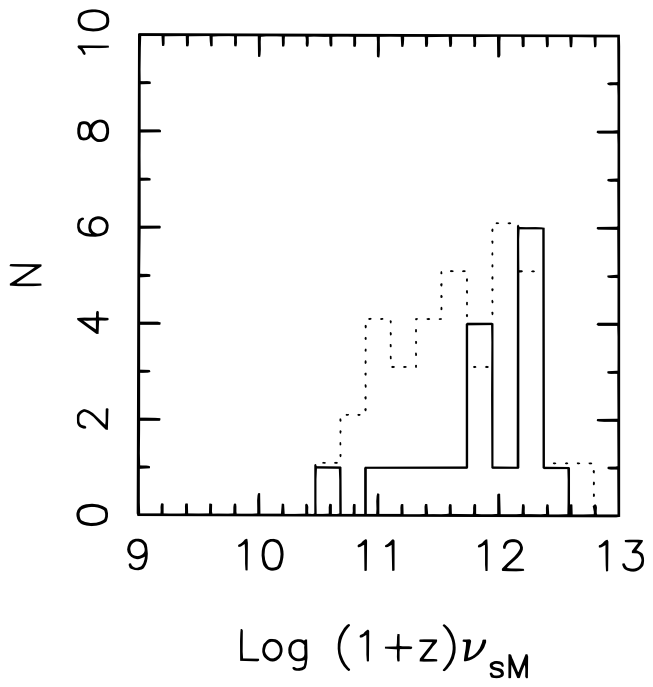

FIG. 5a

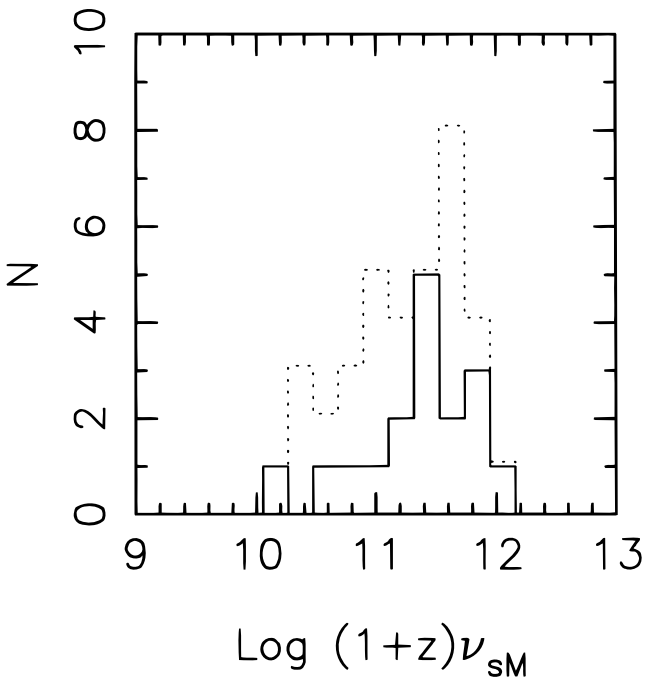

FIG. 5b

FIG. 5.—Distributions of the turnover frequency $\nu_{sM}(1 + z)$ in the source rest frame for the EGRET sources (*solid histograms*) and all other sources in the sample (*dotted histograms*), derived from (*a*) model A and (*b*) model C, respectively.

sources (Ghisellini et al. 1993). The proper-motion data are not taken into account in the derivation of the Doppler factor δ in the homogeneous sphere model. In our model, the proper-motion information is used in the derivation of both the Doppler factor δ and the Lorentz factor γ. We suggest that the homogeneous sphere model could be particularly useful for sources without data for proper motion.

4.4. *Correlation of Relative γ-Ray Luminosity with Doppler Factor δ*

Recently, about 50 AGNs have been detected in high-energy γ-ray emission by EGRET (von Montigny et al. 1995; Thompson et al. 1995). Seventeen EGRET sources are listed in our sample. We present the correlation of the

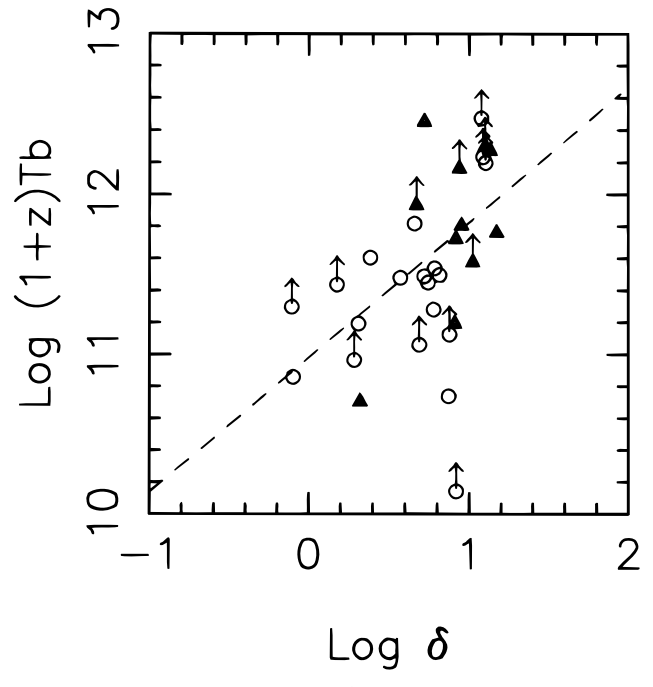

FIG. 6a

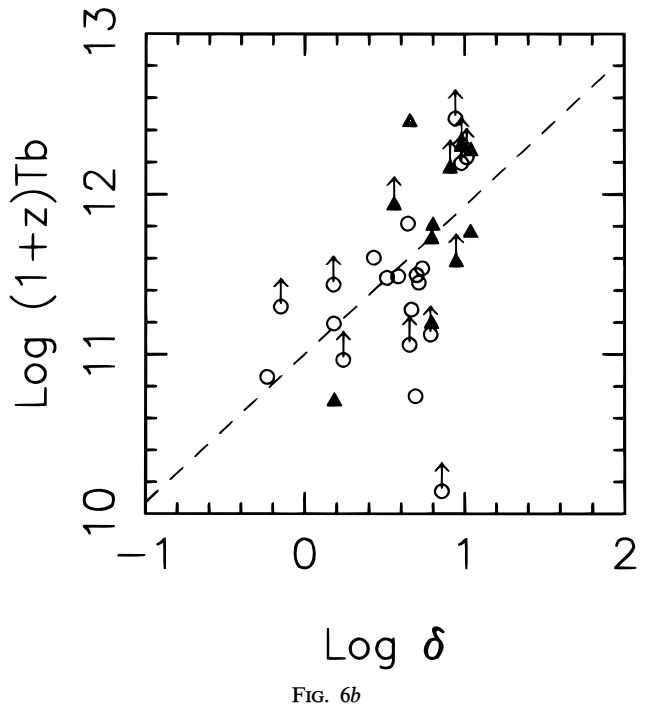

FIG. 6b

FIG. 6.—The intrinsic brightness temperature in the source rest frame vs. the Doppler factor δ derived from (*a*) model A and (*b*) model C, respectively. Arrows indicate the low limits on the brightness temperature.

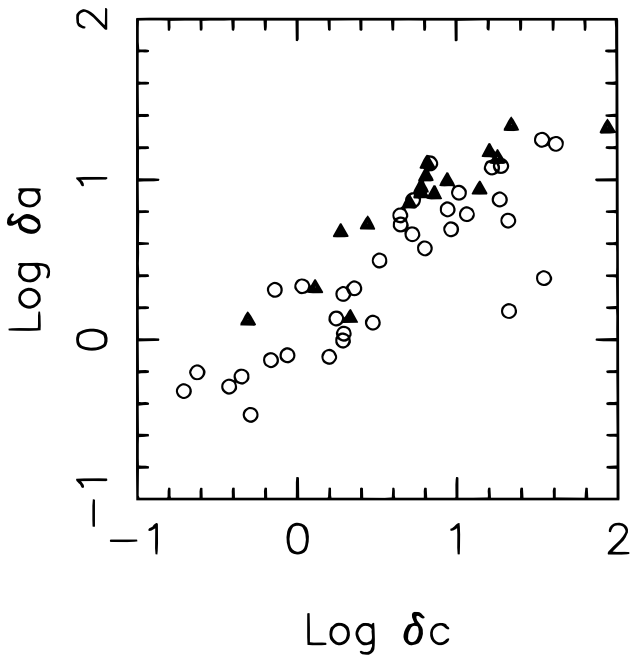

FIG. 7.—Doppler factor δ derived from model A vs. that derived from model C. *Triangles*: EGRET sources; *circles*: all other sources.

relative γ-ray luminosity L_γ with the Doppler factor δ in Figure 8*a*. The relative γ-ray luminosity L_γ is simply defined by $L_\gamma = d_L^2 F$, where d_L is the luminosity distance and F is the maximum photon flux in γ-ray range, taken from von Montigny et al. (1995) and Thompson et al. (1995). The best correlations for the data derived from models A and B are $\log L_\gamma = -1.80 + 2.45 \log \delta$ (at the 99.9% level) and $\log L_\gamma = -1.59 + 2.52 \log \delta$ (at the 99.9% level), respectively. We find the correlation $\log L_\gamma = -0.94 + 1.58 \log \delta$ (at the 99.9% level) for model C, plotted in Figure 8*b*.

5. DISCUSSION

We summarize the main results obtained in the previous sections as follows:

1. The values of the Doppler factor δ of the EGRET sources are higher than those of the non-EGRET sources in our sample, except for three BL Lacs, Mrk 421, 0716+714, and 1219+285, although some sources other than the EGRET sources also have high δ. The values of the Lorentz factor γ of the EGRET sources show similar behavior.
2. The EGRET sources, except the three BL Lacs, have both large values of the Lorentz factor γ (≥ 10) and δ ($\delta \geq \delta_c$, $\delta_c = 4.5$, 3.5, for models A and B, respectively), which seems to be the significant difference between the EGRET and the remaining sources in the sample.
3. The derived turnover frequency $(1 + z)\nu_{sM}$ measured in the source rest frame are higher for the EGRET sources than for the rest of the sources in the sample, although some sources other than the EGRET sources still have high turnover frequencies.
4. The BL Lacs have a mean Lorentz factor γ similar to that of the core-dominated quasars, but the mean viewing angle θ of the BL Lacs is slightly larger than that of the core-dominated quasars. The lobe-dominated quasars have a large mean viewing angle, $\sim 40°$, while for the core-dominated quasars it is $\sim 10°$.
5. There are significant correlations between the brightness temperature in the source rest frame $(1 + z)T_b$ and the Doppler factor δ for both models A and B. No similar significant correlation is found for model C.
6. The significant correlations of the relative γ-ray luminosity L_γ are found with the Doppler factor δ for both models A and B.

There are 17 EGRET sources included in our sample. Except for three BL Lacs, all of the remaining 14 EGRET sources show high values of δ and γ. The mean viewing angles for 14 EGRET sources are 4°.9 and 5°.7 for models A

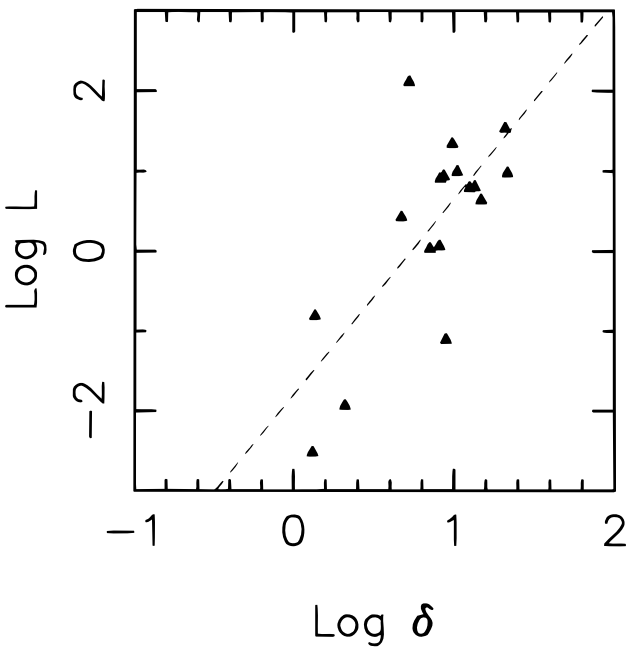

FIG. 8*a*

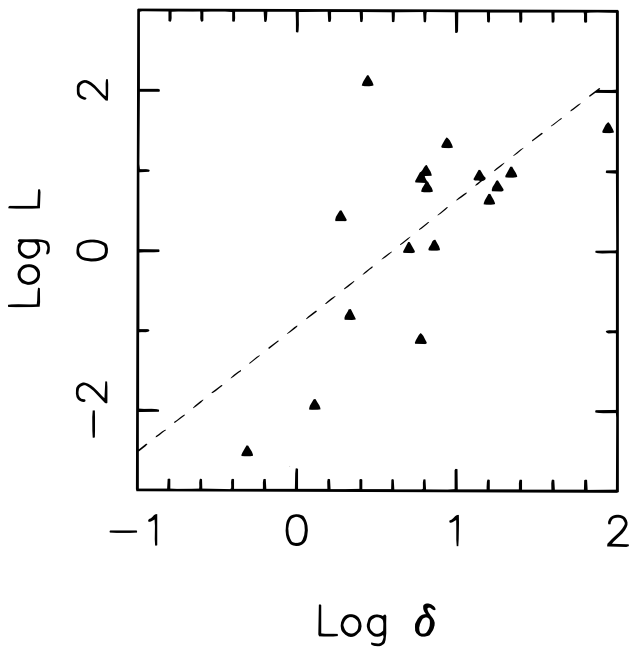

FIG. 8*b*

FIG. 8.—Relative γ-ray luminosity vs. Doppler factor δ, derived from (*a*) model A and (*b*) model C, respectively

and B, respectively. We have not seen any difference in intrinsic physical properties between these two types of sources from our statistical results. These suggest that the γ-ray emissions from the AGNs are mainly due to beaming effects. Only the sources with high Doppler factor δ, which are strongly beamed to us, are detected at γ-ray energies. For the synchrotron self-Compton model of γ-ray production, the Doppler factor δ, rather than the Lorentz factor γ, of the bulk motion of the jet plays a crucial role in the observed γ-ray flux. Sikora, Begelman, & Rees (1993, 1994) have proposed that the γ-ray emission originates in a jet as a product of inverse Compton scattering of relativistic electrons and seed photons produced externally to the jet. Moving in a homogeneous photon "bath" (produced by material scattering photons from the disk, or by the broad-line region), the jet would "see" this radiation energy density amplified by a factor of γ^2. Therefore, in this model the Lorentz factor γ together with Doppler factor δ determine the γ-radiation. The fact that some sources with a high Doppler factor δ and low Lorentz factor γ have not been detected the γ-ray emission might imply that the seed photons are from somewhere outside the jet, if the γ-radiation detected by EGRET is due to the inverse Compton scattering of lower energy photons up to γ-ray energies by beamed relativistic electrons. Thus, sources with low Lorentz factors may not be able to produce sufficient γ-rays through inverse Compton scattering of the external soft photons.

The source $1308+326$ has high δ and γ, similar to the EGRET sources in the sample; yet it is a non-EGRET source. This might be due to the measurements of the value of proper motion. Overestimation of the proper motion of the source would lead to overestimation of its δ and γ. Further VLBI measurements of the proper motion of this object are necessary. The other possibility is that the object is a γ-ray source in a quiescent state, and therefore has not been detected by EGRET.

We cannot see significant differences between the mean values of δ, γ, and θ of the BL Lacs and those of all sources in the sample (Table 3). The mean value of the Lorentz factor γ of the BL Lacs is similar to that of the core-dominated quasars, and the mean viewing angle of BL Lacs is slightly larger than that of the core-dominated quasars. The mean values of Doppler factors show that the core-dominated quasars are more beamed than the BL Lacs. The results obtained here seem not to agree with the previous suggestion that the viewing angles of BL Lacs are smaller. Three BL Lacs, Mrk 421, $0716+714$, and $1210+285$, are quite special, having relatively low Lorentz and Doppler factors and large viewing angles, but being detected at γ-ray energies. One possible reason might be that the BL Lac objects have a different radiation mechanism from the other AGNs. Urry (1994) suggested that the X-ray emission from the BL Lacs is due to synchrotron radiation rather than synchrotron self-Compton radiation. Thus, there may be some problems in using a single model to describe all AGNs.

Table 3 shows that the core-dominated and lobe-dominated quasars have rather different mean values of viewing angle. Therefore, these two types of quasars may be the same phenomenon, but seen at different viewing angles, which is consistent with the previous results (Ghisellini et al. 1993) and the unified scheme.

The correlation between the brightness temperature in the source rest frame, $(1+z)T_b$, and the Doppler factor δ derived in our model suggest that the derived values of beaming parameters are a good approximation. As a comparison, the correlation is less significant for the homogeneous sphere model. However, the homogeneous sphere model is useful for estimating the Doppler factor, especially for objects without proper motion data, since the derived Doppler factor from the homogeneous sphere model is in general compatible with that from our inhomogeneous jet model (see Fig. 7). The correlation of the relative γ-ray luminosity L_γ with the Doppler factor δ presented in Figure 8 strongly suggests that the γ-ray emission from AGNs is beamed, although the detailed mechanism for γ-ray emission is still not clear.

Two sets of the parameters α, m, and n are adopted in the model calculations, and we adopted the same values of these parameters for all sources in one model calculation. In practice, the sources may have different values of the parameters α, m, and n, and in principle these parameters could be constrained by the observable quantities α_{S1}, α_{C2}, and k_m. Unfortunately, this information is only found for a few cases through multifrequency VLBI observations. Further high-resolution multifrequency VLBI observations would be helpful to improve our model calculations.

We thank the referee for his helpful comments and linguistic improvements to the manuscript. The support from Pandeng Plan is gratefully acknowledged. X. C. thanks support from the Shanghai Observatory, the China Post-Doctoral Foundation, and NSFC.

REFERENCES

Biretta, J. A., Zhou, F., & Owen, F. N. 1995, ApJ, 447, 582
Blandford, R. D., & Königl, A. 1979, ApJ, 232, 34
Bloom, S. D., et al. 1994, AJ, 108, 398
Brunner, H., Lamer, G., Worrall, D. M., & Staubert R. 1994, A&A, 287, 436
Chu, H. S., Bååth, L. B., Rantakyrö, F. T., Zhang, F. J., & Nicholson, G. 1996, A&A, 307, 15
Doeleman, S., Rogers, A. E. E., & Moran, J. M. 1994, in Proc. 2nd EVN/JIVE Symp., ed. A. J. Kus, R. T. Schilizzi, K. M. Borkowski, & L. I. Gurvits (Torun: Torun Radio Astron. Obs.), 39
Gabuzda, D. C., Cawthorne, T. V., Roberts, D. H., & Wardle, J. F. C. 1992, ApJ, 388, 40
Gabuzda, D. C., Mullan, C. M., Cawthorne, T. V., Wardle, J. F. C., & Roberts, D. H. 1994, ApJ, 435, 140
Ghisellini, G., Padovani, P., Celotti, A., & Maraschi, L. 1993, ApJ, 407, 65
Güijosa, A., & Daly, R. A. 1996, ApJ, 461, 600
Hutter, D. J., & Mufson, S. L. 1986, ApJ, 301, 50
Kellerman, K. I., et al. 1977, ApJ, 211, 658
Königl, A. 1981, ApJ, 243, 700
Krichbaum, T. P., et al. 1994, in Proc. 2nd EVN/JIVE Symposium, ed. A. J. Kus, R. T. Schilizzi, K. M. Borkowski, & L. I. Gurvits (Torun: Torun Radio Astron. Obs.), 47
Ku, W. H. M., Helfand, D. J., & Lucy, L. B. 1980, Nature, 288, 323
Lamer, G., Brunner, H., & Staubert, R. 1996, A&A, 311, 384
Marscher, A. P. 1987, ApJ, in Superluminal Radio Sources, ed. J. A. Zensus & T. J. Pearson (Cambridge: Cambridge Univ. Press), 280
Moellenbrock, G. A., et al. 1996, AJ, 111, 2174
Mufson, S. L., Hutter, D. J., & Kondo, Y. 1989, in BL Lac Objects, ed. L. Maraschi, T. Maccacaro, & M.-H. Ulrich (Berlin: Springer), 341
Mutel, R. L. 1990, in Parsec-Scale Radio Jets, ed. J. A. Zensus & T. J. Pearson (Cambridge: Cambridge Univ. Press), 98
Padovani, P. 1992, A&A, 256, 399
Padovani, P., Giommi, P., & Fiore, F. 1997, MNRAS, 284, 569
Padovani, P., & Urry, C. M. 1992, ApJ, 387, 449

Pearson, T. J., & Readhead, A. C. S. 1988, ApJ, 328, 114
Porcas, R. W. 1987, in Superluminal Radio Sources, ed. A. Zensus, & T. Pearson (Cambridge: Cambridge Univ. Press), 12
Rantakyrö, F. T., Bååth, L. B., Dallacasa, D., Jones, D. L., & Wehrle, A. E. 1996, A&A, 310, 66
Readhead, A. C. S. 1994, ApJ, 426, 51
Reich, W., et al. 1993, A&A, 273, 65
Shen, Z. Q. 1996, Ph.D. thesis, Shanghai Observatory
Sikora, M., Begelman, M. C., & Rees, M. J. 1993, in AIP Proc. 280, Compton Gamma-ray Observatory, ed. M. Friedlander, N. Geherels, & D. J. Macomb (New York: AIP), 598
———. 1994, ApJ, 421, 153
Thompson, D. J., et al. 1995, ApJS, 101, 259
Unwin, S. C., Wehrle, A. E., Urry, C. M., Gilmore, D. M., Barton, E. J., Kierulf, B. C., Zensus, J. A., & Rabaca, C. R. 1994, ApJ, 432, 103
Urry, C. M. 1994, in Frontiers of Space and Ground-based Astronomy, ed. W. Wamsteker, M. S. Longair, & Y. Kondo (Dordrecht: Kluwer), 335
Vermeulen, R. C., Bernstein, R. A., Hough, D. H., & Readhead, A. C. S. 1993, ApJ, 417, 541
Vermeulen, R. C., & Cohen, M. H. 1994, ApJ, 430, 467
von Montigny, C., et al. 1995, ApJ, 440, 525
Webb, J. R., et al. 1994, ApJ, 422, 570
Wilkes, B. J., et al. 1994, ApJS, 92, 53
Zensus, J. A. 1989, in BL Lac Objects, ed. L. Maraschi, T. Maccacaro, & M.-H. Ulrich (Berlin: Springer), 3
Zhang, Y. F., Marscher, A. P., Aller, H. D., Aller, M. F., Teräsranta, H., & Valtaoja, E. 1994, ApJ, 432, 91